

# 1 **MUTATE: A Human Genetic Atlas of Multi-organ AI** 2 **Endophenotypes using GWAS Summary Statistics**

3  
4 Alex Boquet-Pujadas<sup>1</sup>, Jian Zeng<sup>2</sup>, Ye Ella Tian<sup>3</sup>, Zhijian Yang<sup>4</sup>, Li Shen<sup>5</sup>, Andrew Zalesky<sup>3</sup>,  
5 Christos Davatzikos<sup>6</sup>, Junhao Wen<sup>1\*</sup>,

6  
7 <sup>1</sup>Laboratory of AI and Biomedical Science (LABS), University of Southern California, Los Angeles, California,  
8 USA

9 <sup>2</sup>Institute for Molecular Bioscience, University of Queensland, Brisbane, QLD 4072, Australia

10 <sup>3</sup>Melbourne Neuropsychiatry Centre, Department of Psychiatry, Melbourne Medical School, The University of  
11 Melbourne, Melbourne, Victoria, Australia

12 <sup>4</sup>GE Healthcare, Bellevue, WA, USA

13 <sup>5</sup>Department of Biostatistics, Epidemiology and Informatics, University of Pennsylvania Perelman School of  
14 Medicine, Philadelphia, PA, USA

15 <sup>6</sup>Artificial Intelligence in Biomedical Imaging Laboratory (AIBIL), Center for AI and Data Science for Integrated  
16 Diagnostics (AI<sup>2</sup>D), Perelman School of Medicine, University of Pennsylvania, Philadelphia, USA

17  
18 \*Corresponding authors:

19 Junhao Wen, [junhao.wen89@gmail.com](mailto:junhao.wen89@gmail.com)

20 2025 Zonal Ave, Los Angeles, CA 90033, United States

## 21 **Abstract**

22 Artificial intelligence (AI) has been increasingly integrated into imaging genetics to provide  
23 intermediate phenotypes (i.e., endophenotypes) that bridge the genetics and clinical  
24 manifestations of human disease. However, the genetic architecture of these AI endophenotypes  
25 remains largely unexplored in the context of human multi-organ system diseases. Using publicly  
26 available GWAS summary statistics from UK Biobank, FinnGen, and the Psychiatric Genomics  
27 Consortium, we comprehensively depicted the genetic architecture of 2024 multi-organ AI  
28 endophenotypes (MAEs). Two AI- and imaging-derived subtypes<sup>1</sup> showed lower polygenicity  
29 and weaker negative selection effects than schizophrenia disease diagnoses<sup>2</sup>, supporting the  
30 endophenotype hypothesis<sup>3</sup>. Genetic correlation and Mendelian randomization analyses reveal  
31 both within-organ relationships and cross-organ interconnections. Bi-directional causal  
32 relationships were established between chronic human diseases and MAEs across multiple organ  
33 systems, including Alzheimer's disease for the brain, diabetes for the metabolic system, asthma  
34 for the pulmonary system, and hypertension for the cardiovascular system. Finally, we derived  
35 polygenic risk scores for the 2024 MAEs for individuals not used to calculate MAEs and  
36 returned these to the UK Biobank. Our findings underscore the promise of the MAEs as new  
37 instruments to ameliorate overall human health. All results are encapsulated into the MUTATE  
38 genetic atlas and are publicly available at <https://labs-laboratory.com/mutate>.

## 39 Introduction

40 Multi-organ research<sup>1,4-11</sup> represents a pivotal frontier in advancing our understanding of human  
41 aging and disease. In particular, integrating artificial intelligence (AI) into multi-organ imaging  
42 genetics<sup>1,4,12,6</sup> has emerged as a novel approach, offering potential promise in advancing  
43 precision medicine<sup>13</sup>. This integration introduces a new array of endophenotypes<sup>14,15</sup>, serving as  
44 intermediate, often quantitative, phenotypes, potentially reshaping how we perceive and  
45 approach medical AI<sup>16</sup> in imaging and genetic research.

46 In recent years, three primary catalysts have significantly advanced the field of genetics.  
47 The first pivotal factor stems from the extensive collaborative efforts in consolidating large-scale  
48 multi-omics datasets, which has endowed researchers with unprecedented statistical power  
49 previously inaccessible. As an illustration, the UK Biobank (UKBB) study<sup>17</sup> stands out for its  
50 comprehensive collection of multi-organ imaging<sup>18</sup>, genetics<sup>19</sup>, and proteomics<sup>20,21</sup> data within  
51 the United Kingdom. Similarly, the FinnGen study<sup>22</sup>, conducted in Finland, has amassed  
52 extensive clinical and genetic data. Secondly, efforts toward open science have propelled the  
53 field, especially emphasizing the significance of publicly available resources, such as genome-  
54 wide association study (GWAS) summary statistics and widespread scientific dissemination.  
55 Notably, the FinnGen study and Psychiatric Genomics Consortium (PGC<sup>23</sup>) have publicly made  
56 all the GWAS summary statistics accessible<sup>22</sup>. Public GWAS platforms such as the GWAS  
57 Catalog<sup>24</sup>, OpenGWAS<sup>25</sup>, and GWAS ATLAS<sup>26</sup> have consolidated and harmonized vast GWAS  
58 datasets, rendering them suitable for subsequent genetic analyses. Likewise, such good practice  
59 was also employed in the newly burgeoning field of brain imaging genetics<sup>27</sup>, including the  
60 BIG40 (<https://open.win.ox.ac.uk/ukbiobank/big40/>), the BIG-KP (<https://bigkp.org/>),  
61 BRIDGEPORT (<https://labs-laboratory.com/bridgeport>), and MEDICINE (<https://labs-laboratory.com/medicine>)  
62 knowledge portals. Finally, advanced computational genomics  
63 statistical methods using solely GWAS summary statistics, along with sufficient linkage  
64 disequilibrium information, have been developed, presenting an unparalleled chance to  
65 comprehend the genetic architecture of highly polygenic disease traits. For example, LDSC<sup>28</sup> has  
66 been extensively utilized to estimate single-nucleotide polymorphism (SNP)-based heritability  
67 and genetic correlations. Mendelian randomization<sup>29</sup> is a statistical method to dissect associations  
68 further, probing potential causal relationships among these complex human disease traits,  
69 although these methods often rely on several sensitive model assumptions<sup>30</sup>.

70 Despite these advancements, the intricate genetic foundation shaping these AI  
71 endophenotypes in the context of pleiotropic human disease endpoints (DE) within multi-organ  
72 systems remains largely uncharted. We previously applied AI to imaging genetic data and  
73 derived 2024 multi-organ AI endophenotypes (MAE). These encompassed 2003 multi-scale  
74 brain patterns of structural covariance (PSC) networks generated through a deep learning-  
75 analogy non-negative matrix factorization method<sup>12</sup> (visualization for C32\_1 encompassing deep  
76 subcortical structures: [https://labs-laboratory.com/bridgeport/MuSIC/C32\\_1](https://labs-laboratory.com/bridgeport/MuSIC/C32_1)), 9 dimensional  
77 neuroimaging endophenotypes (DNE) quantifying neuroanatomical heterogeneity (also known as  
78 disease subtype) within 4 common brain diseases<sup>7</sup>, and 12 biological age gap (BAG) assessing  
79 the individual deviation in typical aging (i.e., acceleration or deceleration from the chronological  
80 age) across 9 human organ systems<sup>4,6</sup> (**Supplementary eTable 1a**). To contribute to open  
81 science<sup>31</sup>, we made all the GWAS summary statistics derived from UKBB data publicly  
82 available at the MEDICINE knowledge portal: <https://labs-laboratory.com/medicine>. In addition,  
83 FinnGen analyzed genetic data for 2269 binary and 3 quantitative DEs from 377,277 individuals  
84 and 20,175,454 variants. They made these massive GWAS summary statistics publicly available

85 to the community at <https://finngen.gitbook.io/documentation/> (**Supplementary eTable 1b**).  
86 Finally, PGC consolidated GWAS results focused on neurological disorders worldwide and  
87 made the GWAS summary statistics accessible to the research community (<https://pgc.unc.edu/>,  
88 **Supplementary eTable 1c**).

89 This study harnesses the extensive GWAS summary resources made publicly available  
90 by us on behalf of UKBB, FinnGen, and PGC (**Method 1**), along with the utilization of several  
91 advanced computational genomics statistical methods (refer to **Code Availability**), to thoroughly  
92 depict the genetic architecture of the 2024 MAEs (**Method 2**) and 525 DEs (>5000 cases) in the  
93 context of multi-organ investigations. Importantly, our previous research explored the genetic  
94 foundation of the 2024 MAEs but did not systematically encompass the FinnGen or PGC data.  
95 Specifically, we included 521 DEs released by the FinnGen study, accessible at  
96 <https://finngen.gitbook.io/documentation/v/r9/>, and 4 brain DEs (Alzheimer’s disease (AD),  
97 Attention-deficit/hyperactivity disorder (ADHD), bipolar disorder (BIP), and schizophrenia  
98 (SCZ)) from PGC (<https://pgc.unc.edu/>). This study expanded on this by systematically  
99 benchmarking the genetic analyses and comprehensively comparing various statistical  
100 methodologies<sup>28,30,32–38</sup> (**Method 3**). Specifically, we aimed to compute the SNP-based  
101 heritability ( $h_{SNP}^2$ ), polygenicity ( $\pi$ ), the relationship between SNP effect size and minor allele  
102 frequency ( $S$ : signature of natural selection, genetic correlation ( $r_g$ ), causality, and polygenic risk  
103 score (PRS) between the 2024 MAEs and 525 DEs. These findings were encapsulated within the  
104 MUTATE (**MUITi-organ AI endophenoTypeE**) genetic atlas, which is publicly available at  
105 <https://labs-laboratory.com/mutate>.

## 106 Results

### 107 The genetic architecture of the 2024 MAEs and 525 DEs

108 We computed three parameters to fully depict the genetic architecture of the 2024 MAEs  
109 (**Method 3a**). For the SNP-based heritability ( $h_{SNP}^2$ ), SBayesS<sup>39</sup> obtained the highest  $h_{SNP}^2$  for the  
110 2016 brain MAEs (mean  $\hat{h}_{SNP}^2=0.13$  [0.01, 0.38]), followed by the pulmonary BAG  
111 ( $0.16\pm 0.004$ ), the eye BAG ( $0.14\pm 0.009$ ), the cardiovascular BAG ( $0.12\pm 0.003$ ), the renal BAG  
112 ( $0.10\pm 0.003$ ), and the musculoskeletal BAG ( $0.10\pm 0.003$ ) (**Fig. 1a** and **Supplementary eFile 1**).  
113 It is worth noting that SNP-based heritability varies across methods and depends on the input  
114 data, i.e., summary data or individual-level genotype data used in the method<sup>40</sup>. We aimed to  
115 benchmark the summary data-based methods by comparing the results from SBayesS with those  
116 of LDSC<sup>28</sup> and SumHer<sup>33</sup>. Overall, while the estimates from the three methods were highly  
117 correlated ( $r=0.97$  between LDSC and SumHer;  $r=0.99$  between SBayesS and SumHer;  $r=0.99$   
118 between SBayesS and LDSC; **Supplementary eFigure 1**), SumHer ( $0.23\pm 0.14$ ) generally  
119 yielded larger  $h_{SNP}^2$  estimates than both LDSC ( $0.16\pm 0.10$ ) and SBayesS ( $0.13\pm 0.08$ )  
120 (**Supplementary eFile 1**). We present the  $h_{SNP}^2$  estimate of the 525 DEs and 2024 MAEs in  
121 **Supplementary eFigure 2**. **Supplementary eFile 2** presents the results of the 525 DEs. For the  
122 525 DEs, we converted the  $h_{SNP}^2$  estimates from the observed scales to the liability scales,  
123 following the recommendations of Ojavee et al<sup>41</sup>. It's important to clarify that we did not intend  
124 to compare the  $h_{SNP}^2$  estimates of the two data sources due to differences in genotype coverage,  
125 sample sizes, allele frequencies, and other factors.

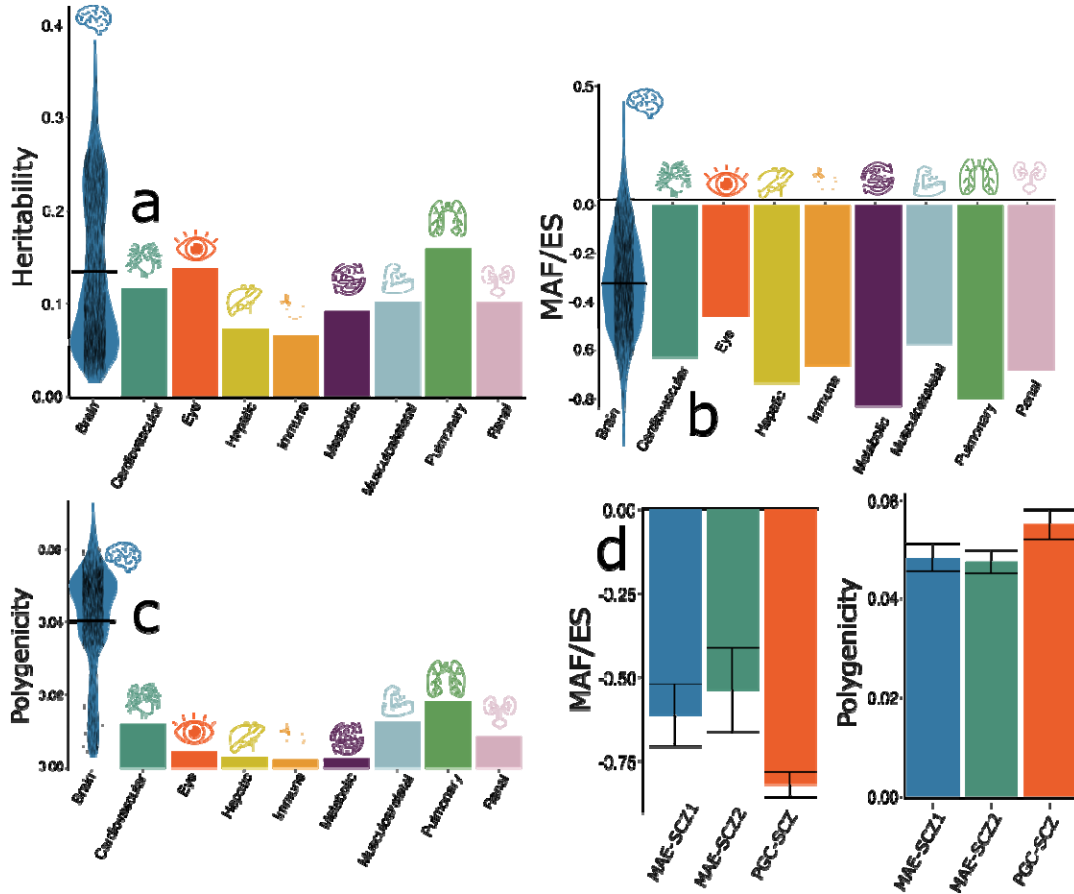
126 We then computed the natural selection signature ( $S$ ) for the 2024 MAEs. The metabolic  
127 BAG showed a strong negative selection ( $S=-0.82\pm 0.10$ ), followed by the pulmonary BAG ( $S=-$   
128  $0.79\pm 0.05$ ), the hepatic BAG ( $S=-0.74\pm 0.09$ ), the renal BAG ( $S=-0.68\pm 0.08$ ), and the immune  
129 BAG ( $S=-0.66\pm 0.11$ ). For the brain MAEs ( $S=-0.33$  [-1, 0.43]), the brain BAG and ( $S=-$   
130  $0.70\pm 0.12$ ) the subtype (ASD1) for autism spectrum disorder<sup>42</sup> ( $S=-0.90\pm 0.11$ ) showed strong  
131 negative selection effects (**Fig. 1b** and **Supplementary eFile 3**).

132 Finally, we calculated the polygenicity ( $\pi$ ) for the 2024 MAEs. We found that brain  
133 MAEs ( $0.040$  [0.003, 0.072]) showed higher polygenicity than other organ systems (t-  
134 statistic=5.75; P-value= $1.03\times 10^{-8}$ ), followed by the pulmonary BAG ( $0.018\pm 0.001$ ), the  
135 musculoskeletal BAG ( $0.013\pm 0.001$ ), and the cardiovascular BAG ( $0.011\pm 0.001$ ) (**Fig. 1C** and  
136 **Supplementary eFile 4**). The PSC (C128\_115: [https://labs-](https://labs-laboratory.com/bridgeport/MuSIC/C128_115)  
137 [laboratory.com/bridgeport/MuSIC/C128\\_115](https://labs-laboratory.com/bridgeport/MuSIC/C128_115)) showed the highest polygenicity estimate  
138 ( $0.072\pm 0.002$ ).

### 139 Potential evidence for the endophenotype hypothesis

141 Previous studies<sup>43,44</sup> have found supporting evidence for the endophenotype hypothesis<sup>14,15</sup> using  
142 traditional brain map-based signatures, showing that more genetic variants are associated with  
143 disease endpoints than imaging-derived signatures (i.e., endophenotypes). Of note, considering  
144 genetic differences between FinnGen and UKBB samples, SBayesS with the UKBB as LD  
145 reference may give biased estimates of  $S$  and  $\pi$  (LD from FinnGen not fully available; **Method**  
146 **3a**). Therefore, we used the GWAS summary data for PGC schizophrenia (SCZ<sup>2</sup>) and two  
147 subtypes of SCZ (SCZ1 and SCZ2<sup>1</sup>) from our UKBB analysis to demonstrate this. The  
148 advantage of using PGC data is that the GWAS summary statistics are better powered (large  
149 sample sizes), and the data were from European ancestry groups across different countries. A  
150 data harmonization procedure is outlined in **Supplementary eMethod 1** to ensure a fair

151 comparison of these estimates, which led to the utilization of a common set of SNPs and linkage  
 152 disequilibrium information for computing the  $S$  and  $\lambda$  parameters. Our results showed that MAE-  
 153 SCZ1 ( $\lambda = -0.048 \pm 0.002$ ;  $S = -0.61 \pm 0.09$ ) and MAE-SCZ2 ( $\lambda = -0.047 \pm 0.002$ ;  $S = -0.54 \pm 0.12$ ) had  
 154 lower polygenicity signals and weaker negative selection effects than PGC-SCZ  
 155 ( $\lambda = -0.055 \pm 0.003$ ;  $S = -0.82 \pm 0.04$ ) (**Fig. 1d**). **Supplementary eFigure 3** shows the Manhattan plot  
 156 of the harmonized summary data for MAE-SCZ1, MAE-SCZ2, and PGC-SCZ. These findings  
 157 potentially support the endophenotype hypothesis<sup>3</sup>, which suggests that intermediate phenotypes  
 158 (e.g., SCZ subtype MAEs) reside inside the causal pathway from genetics to exo-phenotypes  
 159 (e.g., SCZ binary diagnosis), making them closer to the underlying etiology<sup>43,44</sup>.



160  
 161 **Figure 1: The genetic architecture of the 2024 MAEs**

162 Three parameters are estimated by SBayesS to delineate the genetic architecture of the 2024  
 163 MAEs, including (a) the SNP-based heritability ( $h^2$ ), (b) the relationship between MAF and  
 164 effect size ( $S$ ), and (c) polygenicity ( $\lambda$ ). (d) We compared the  $\lambda$  and  $S$  parameters using  
 165 harmonized GWAS summary data for two AI- and imaging-derived subtypes (MAE-SCZ1 and  
 166 MAE-SCZ2<sup>1</sup>) from UKBB and the disease endpoint of schizophrenia (PGC-SCZ<sup>2</sup>) from PGC.  
 167 FinnGen data was not used due to bias stemming from the unavailability of FinnGen-specific  
 168 linkage disequilibrium data (**Supplementary eMethod 1**). We present the distribution of the  
 169 estimated parameters for the 2016 brain MAEs using a violin plot; the mean value is denoted by  
 170 the black horizontal line. These results should be interpreted cautiously for comparative purposes  
 171 due to limitations stemming from the lack of individual genotype data from FinnGen and PGC,  
 172 differing linkage disequilibrium structures, and varying sample sizes.

173



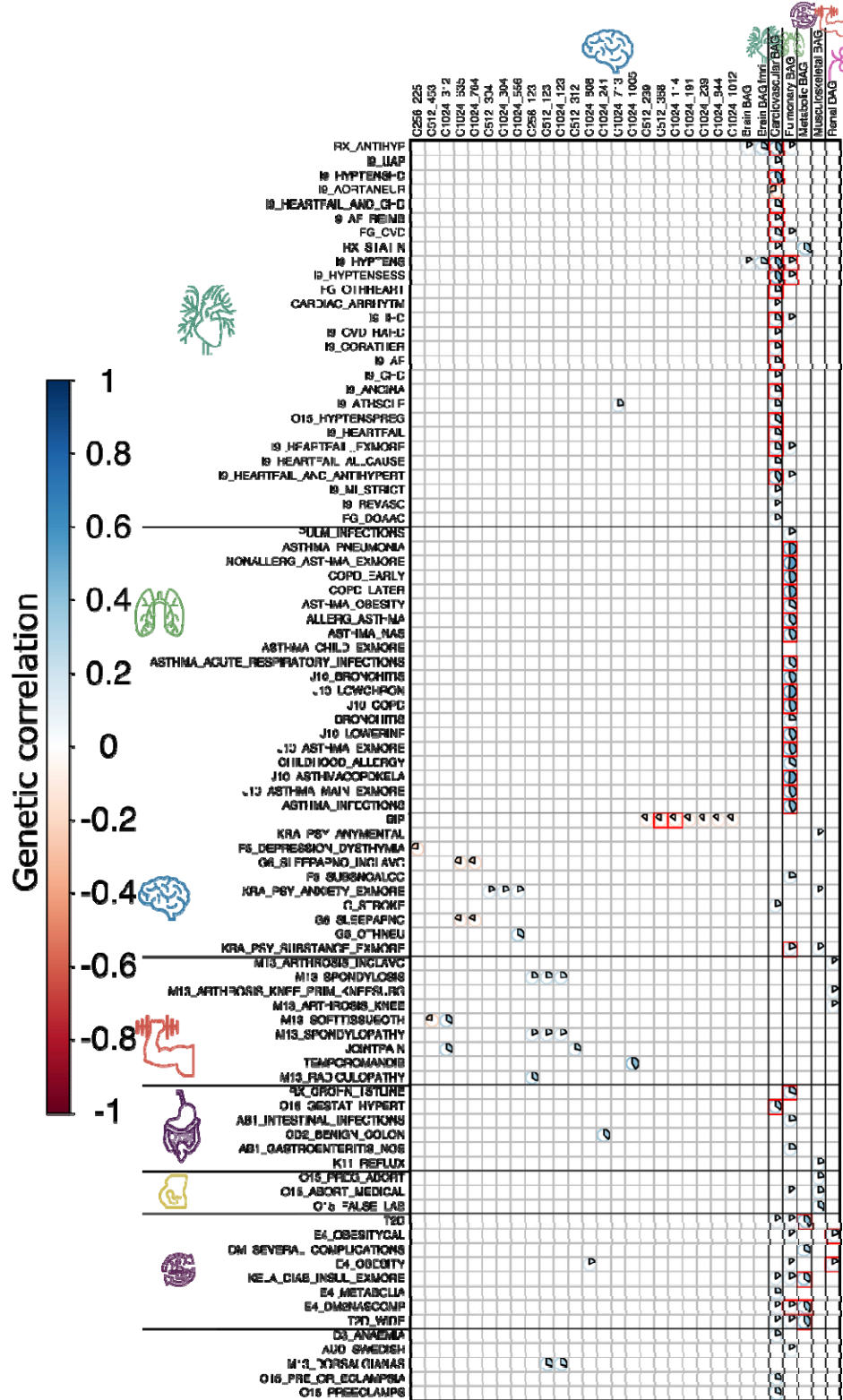
174 **The genetic correlation shows organ-specific and cross-organ associations**

175 We found 132 (P-value < 0.05/2024) and 45 (P-value < 0.05/2024/525) commonly significant  
176 positive genetic correlations ( $r_g$ ) after applying two levels of Bonferroni correction (**Fig. 2**) for  
177 the LDSC<sup>28</sup> and GNOVA<sup>34</sup> methods (**Method 3b**, **Supplementary eFile 5**, and **Supplementary**  
178 **eTable 2**). We noted that HDL encountered convergence issues with the models, as detailed in  
179 **Method 3b**.

180 Between these methods, the magnitude of the genetic correlations for the significant  
181 signals for both methods differed: mean  $\hat{r}_g=0.24[-0.40\sim0.52]$  with 213 significant signals for  
182 LDSC, mean  $\hat{r}_g=0.17[-0.30\sim0.62]$  for GNOVA with 428 significant signals (**Fig. 2**). The three  
183 sets of converged estimates showed a strong correlation:  $r=0.77$  (P-value< $1\times10^{-10}$ ;  $N=1,062,577$ )  
184 between LDSC and GNOVA,  $r=0.81$  (P-value< $1\times10^{-10}$ ;  $N=59,289$ ) between LDSC and HDL,  
185 and  $r=0.82$  (P-value< $1\times10^{-10}$ ;  $N=59,289$ ) between GNOVA and HDL. **Supplementary eFigure**  
186 **4** shows the correlation of the three sets of estimates.

187 Within the significant signals identified, we observed *i*) organ-specific associations, in  
188 which the MAE showed a genetic association with the DE originating from the respective organ  
189 system, and *ii*) cross-organ connections, in which the MAE and DE were primarily involved  
190 from different organ systems. For example, two brain PSCs showed significant negative genetic  
191 correlations with BIP from PGC (C512\_368 vs. BIP:  $-0.16\pm0.03$ ; C1024\_114 vs. BIP: -  
192  $0.15\pm0.03$ ). At a less stringent level, the brain MAEs were also genetically associated with DEs  
193 from other organ systems, including the positive correlation between C1024\_808 and obesity  
194 (E4\_OBESITY:  $r_g=0.17\pm0.13$ ). The cardiovascular BAG was positively correlated with several  
195 DEs related to the cardiovascular system, including ischemic heart disease (I9\_IHD:  
196  $r_g=0.26\pm0.03$ ), coronary heart disease (I9\_HEARTFAIL\_AND\_CHD:  $r_g=0.26\pm0.03$ ), angina  
197 (I9\_ANGINA:  $r_g=0.25\pm0.03$ ) and atrial fibrillation (I9\_AAF:  $r_g=0.22\pm0.04$ ). Likewise, the  
198 pulmonary BAG was positively associated with multiple DEs related to the lung and respiratory  
199 system, including chronic obstructive pulmonary disease (COPD\_EARLY:  $r_g=0.47\pm0.04$ ) and  
200 various forms of asthma (ASTHMA\_NAS:  $r_g=0.43\pm0.04$ ). Cross-organ connections were  
201 established, such as between the pulmonary BAG and substance abuse  
202 (KRA\_PSY\_SUBSTANCE\_EXMORE:  $r_g=0.20\pm0.03$ ) and hypertension (I9\_HYPTENS:  
203  $r_g=0.17\pm0.03$ ). Lastly, the metabolic BAG was largely linked to different forms of diabetes  
204 (T2D:  $r_g=0.40\pm0.04$ ).

It is made available under a [CC-BY-ND 4.0 International license](https://creativecommons.org/licenses/by-nd/4.0/).



205  
 206 **Figure 2: Genetic correlation between the 2024 MAEs and 525 DEs**  
 207 The significant genetic correlation estimates ( $r_g$ ) between 2024 MAEs and 525 DEs are depicted,  
 208 considering two levels of corrections for multiple comparisons, considering the relatively smaller  
 209 sample sizes (<40,000) for brain MAEs compared to other organ MAEs (>100,000). Initially, we



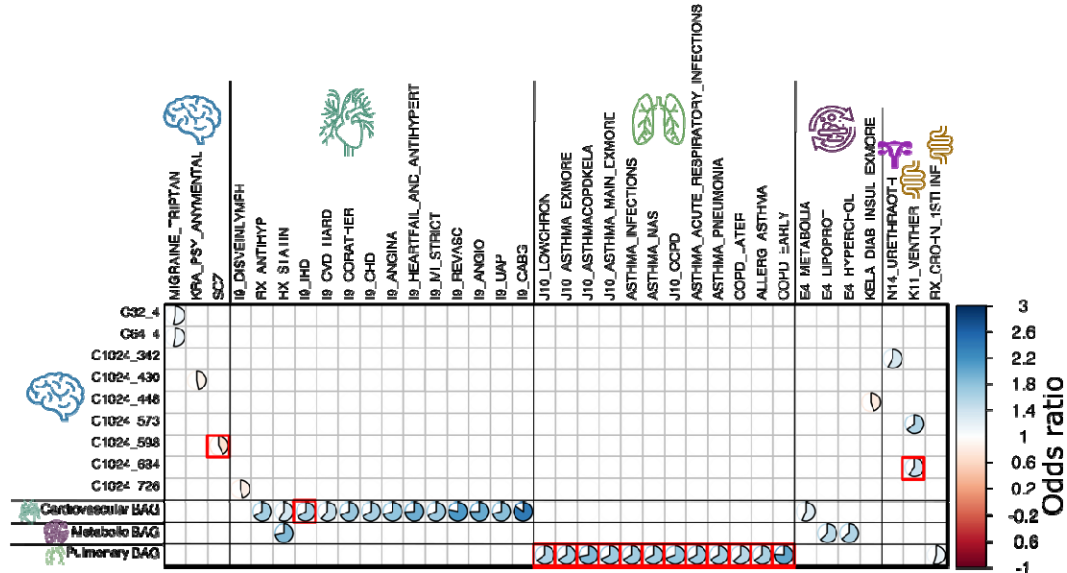
210 reveal significant results shared between LDSC and GNOVA, employing Bonferroni correction  
211 based solely on the number of MAEs (P-value<0.05/2024), uncovering 133 MAE-AE pairs.  
212 Subsequently, a stricter correction based on both the number of MAEs and DEs is applied,  
213 leading to 45 unique MAE-AE pairs marked as red squares; the numeric results are displayed  
214 using results from LDSC. The genetic correlation for non-significant results was set to 0 for  
215 visualization purposes. For the MAEs, readers can explore the BRIDGEPORT portal for a visual  
216 representation of the 2003 brain PSCs (e.g., C256\_225: [https://labs-](https://labs-laboratory.com/bridgeport/MuSIC/C256_225)  
217 [laboratory.com/bridgeport/MuSIC/C256\\_225](https://labs-laboratory.com/bridgeport/MuSIC/C256_225)) and the other BAGs at the MEDICINE portal:  
218 <https://labs-laboratory.com/medicine>.

### 219 220 **The brain, cardiovascular, and pulmonary MAEs are causally linked to DEs of multiple** 221 **organ systems**

222 Employing five distinct two-sample Mendelian randomization estimators, we identified 39 (P-  
223 value<0.05/633) and 15 (P-value<0.05/633/524) significant causal relationships, directed from  
224 the MAE to DE, that withstood the Bonferroni correction at two different levels of rigors, as per  
225 the inverse variance weighted (IVW) estimator and at least one of the other four estimators  
226 (**Method 3c** and **Supplementary eTable 3**).

227 Within the 15 significant causal relationships, the brain MAEs showed causal  
228 connections with DEs from the brain, as well as DEs from other organ systems. For example, the  
229 brain PSC (C1024\_598) was causally linked to SCZ from PGC [P-value=9.89x10<sup>-8</sup>; OR (95%  
230 CI)=0.69 (0.59, 0.79); the number of IVs=7]. C1024\_684 was causally linked to Ventral hernia  
231 from FinnGen [K11\_VENTHER: P-value=1.09x10<sup>-7</sup>; OR (95% CI)=1.43 (1.25, 1.63); the  
232 number of IVs=18]. The pulmonary BAG was causally linked to multiple DEs related to the  
233 pulmonary system, including chronic obstructive pulmonary disease (COPD) [J10\_COPD: P-  
234 value=2.70x10<sup>-20</sup>; OR (95% CI)=1.77 (1.56, 2.00); the number of IVs=59] and asthma  
235 [ASTHMA\_PNEUMONIA: P-value=1.51x10<sup>-14</sup>; OR (95% CI)=1.67 (1.41, 1.96); the number of  
236 IVs=59]. The cardiovascular BAG was causally linked to ischemic heart disease (IHD)  
237 [ASTHMA\_PNEUMONIA: P-value=1.09x10<sup>-7</sup>; OR (95% CI)=1.64 (1.36, 1.96); the number of  
238 IVs=37] (**Fig. 3**). The quality check of the significant signals is presented in **Supplementary**  
239 **eFolder 1. Supplementary eFile 6** presents the full set of results for the 521 FinnGen DEs and 4  
240 PGC DEs.

241  
242



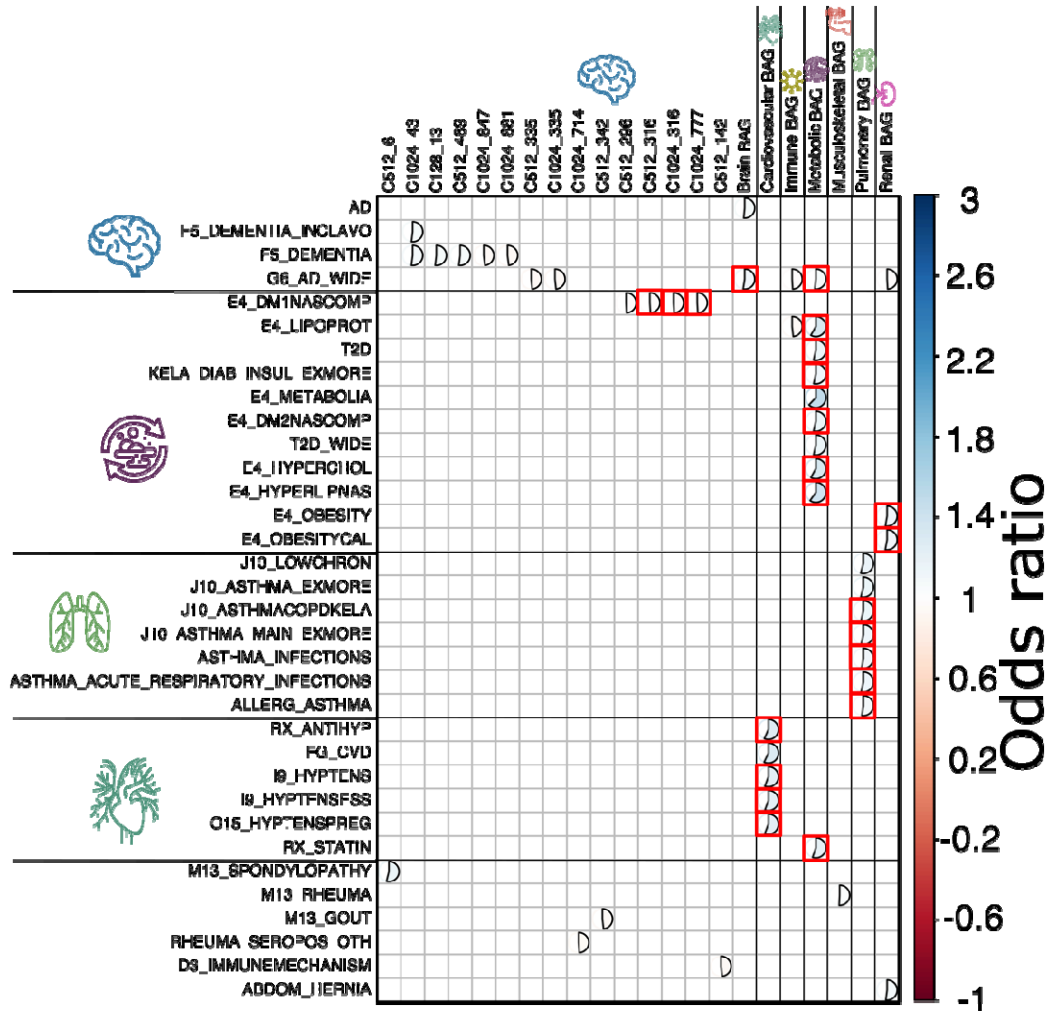
243  
244 **Figure 3: Causal relationship from the 2024 MAEs to the 525 DEs**  
245 The causal relationship from the 2024 MAEs to the 525 DEs revealed 39 significant MAE-DE  
246 pairs, involving 633 MAEs as effective exposure variables (>8 instrumental variables before  
247 harmonization) and 525 DEs as outcomes. Bonferroni correction was applied to identify  
248 potential significant causal signals based on *i*) the 633 MAEs (P-value<0.05/633) and *ii*) the 633  
249 MAEs and 525 DEs (P-value<0.05/633/524, denoted by the 15 red rectangles). Furthermore, we  
250 verified that the statistical significance attained for the IVW estimator was consistent and  
251 persisted across at least one of the other four Mendelian randomization estimators (Egger,  
252 weighted median, simple mode, and weighted mode estimators). For visualization purposes, the  
253 odds ratios for non-significant results were set to 1 and were left blank. For the MAEs, readers  
254 can explore the BRIDGEPORT portal for a visual representation of the 2003 brain PSCs (e.g.,  
255 C32\_4: [https://labs-laboratory.com/bridgeport/MuSIC/C32\\_4](https://labs-laboratory.com/bridgeport/MuSIC/C32_4)) and the other BAGs at the  
256 MEDICINE portal: <https://labs-laboratory.com/medicine>.

257  
258 **The DEs involving Alzheimer’s disease, diabetes, asthma, and hypertension exert causal**  
259 **effects on multi-organ MAEs**

260 We then tested the inverse causality by employing the DEs as exposure and MAEs as outcome  
261 variables. We identified 47 (P-value<0.05/787) and 23 (P-value<0.05/787/214) significant causal  
262 relationships, directed from the DE to MAE, that survived the Bonferroni correction at two  
263 different levels of rigors (**Method 3c** and **Supplementary eTable 4**).

264 Within the 23 significant causal relationships (P-value<0.05/787/214), various forms of  
265 Alzheimer’s disease were linked to the brain MAEs, including the brain BAG [G6\_AD\_WIDE:  
266 P-value=3.03x10<sup>-7</sup>; OR (95% CI)=1.10 (1.06, 1.13); the number of IVs=8] and metabolic BAG  
267 [G6\_AD\_WIDE: P-value=3.03x10<sup>-7</sup>; OR (95% CI)=1.07 (1.04, 1.09); the number of IVs=8].  
268 Type 1 diabetes (E4\_DM1NASCOMP) was also causally linked to multiple brain PSCs. In  
269 addition, the cardiovascular BAG was causally linked to multiple heart diseases, including  
270 hypertension [I9\_HYPTENS: P-value=4.67x10<sup>-31</sup>; OR (95% CI)=1.23 (1.19, 1.27); the number  
271 of IVs=110]. Several forms of asthma were causally linked to the pulmonary BAG, such as  
272 allergic asthma [ALLERG\_ASTHMA: P-value=2.38x10<sup>-9</sup>; OR (95% CI)=1.09 (1.06, 1.13); the  
273 number of IVs=14]. Finally, obesity was also linked to the renal BAG [E4\_OBESITY: P-  
274 value=2.74x10<sup>-8</sup>; OR (95% CI)=1.11 (1.07, 1.15); the number of IVs=19] (**Fig. 4**).

275 **Supplementary eFolder 2** presents the quality check results of the significant signals.  
 276 **Supplementary eFile 7** presents the full set of results for the 521 FinnGen DEs and 4 PGC DEs.  
 277



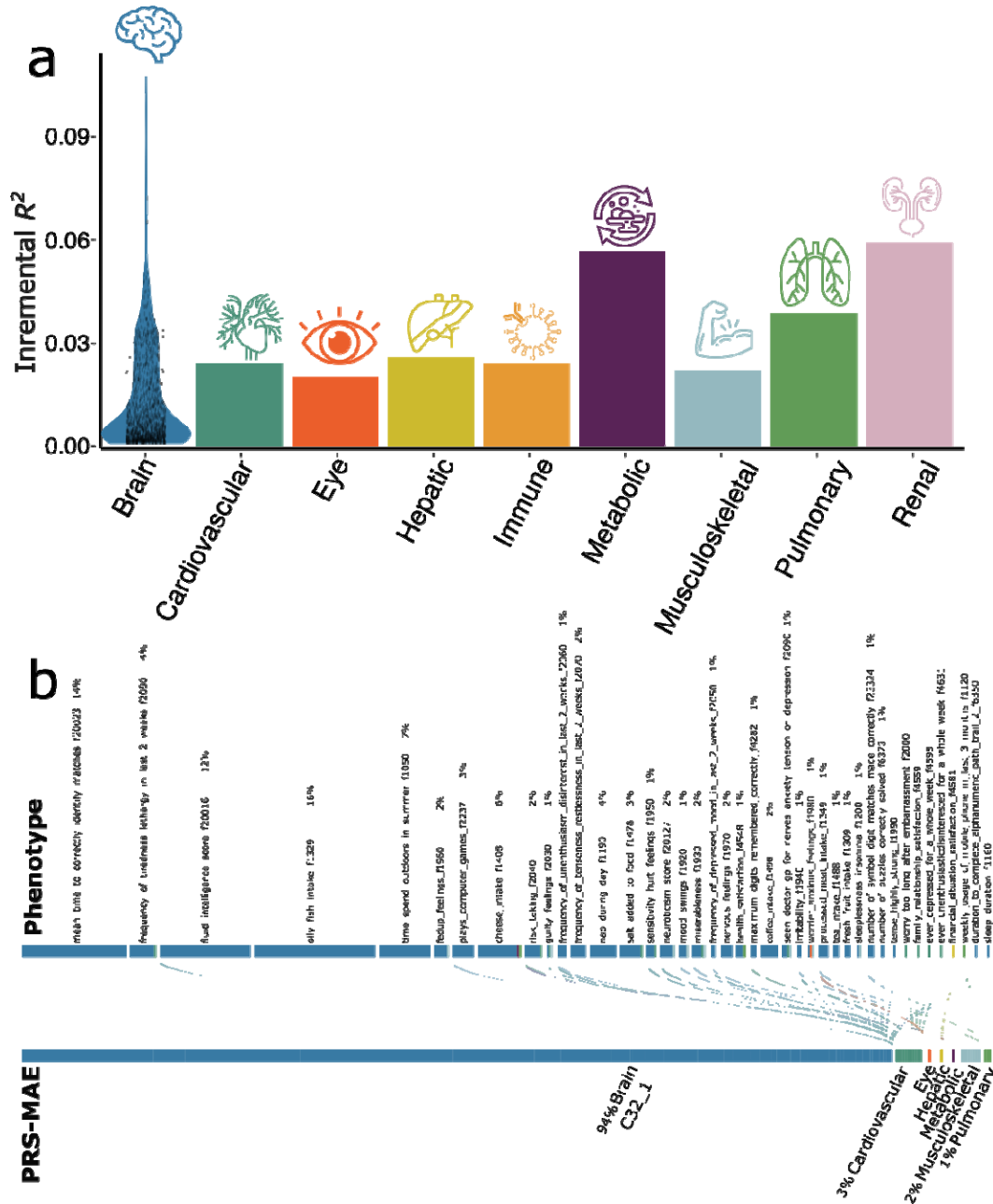
278 **Figure 4: Causal relationship from the 525 DEs to the 2024 MAEs**  
 279 The causal relationship from the 525 MAEs to the 2024 DEs revealed 47 significant DE-MAE  
 280 pairs, involving 214 DEs as effective exposure variables (>8 instrumental variables before  
 281 harmonization) and 787 DEs as effective outcomes after quality checks. Bonferroni correction  
 282 was applied to identify potential significant causal signals based on *i*) the 787 MAEs (P-  
 283 value<0.05/787) and *ii*) the 787 MAEs and 214 DEs (P-value<0.05/787/214, denoted by the 23  
 284 red rectangles). Furthermore, we verified that the statistical significance attained for the IVW  
 285 estimator was consistent and persisted across at least one of the other four Mendelian  
 286 randomization estimators (Egger, weighted median, simple mode, and weighted mode  
 287 estimators). For visualization purposes, the odds ratios for non-significant results were set to 1  
 288 and were left blank. For the MAEs, readers can explore the BRIDGEPORT portal for a visual  
 289 representation of the 2003 brain PSCs (e.g., C128\_13: [https://labs-  
 290 laboratory.com/bridgeport/MuSIC/C128\\_13](https://labs-laboratory.com/bridgeport/MuSIC/C128_13)) and the other BAGs at the MEDICINE portal:  
 291 <https://labs-laboratory.com/medicine>.  
 292

293 **The polygenic risk scores of the 2024 MAEs**  
 294

295 Using the PRS-CS<sup>45</sup> method, we derived the PRS of the 2024 MAEs. We found that the 1799  
296 MAEs could significantly (P-value<0.05/2024) predict the phenotypic BAGs in the test/target  
297 data (split2 GWAS; detailed in **Method 3d**). Among these, 1791 brain MAEs resulted in  
298 significant incremental  $R^2$  ranging from 0.11% to 10.70% to predict the phenotype of interest.  
299 For example, the PSC (C1024\_593 for part of the cerebellum: [https://labs-  
300 laboratory.com/bridgeport/MuSIC/C1024\\_593](https://labs-laboratory.com/bridgeport/MuSIC/C1024_593)) showed an incremental of  $R^2$  10.70%. The renal  
301 BAG showed an incremental  $R^2$  of 5.92%, followed by the metabolic ( $R^2 = 5.67%$ ) and  
302 pulmonary BAG ( $R^2 = 3.86%$ ) (**Fig. 5a** and (**Supplementary eFile 8**)).

303 We then applied the model to the entire UKBB population and performed a PRS-wide  
304 association study (PWAS), where the 2024 PRS-MAEs were linked to the 59 phenotypes that  
305 were not initially used to compute the respective PRS, to avoid the circular bias<sup>46</sup>  
306 (**Supplementary eTable 5**). Refer to **Method 3d** for details. We found 388 significant  
307 associations (P-value<0.05/2024/59) between 7 PRS-MAEs and 41 phenotypes. Among these,  
308 PSC C32\_1 showed the most associations (94%); the lifestyle factor for only fish intake (Field  
309 ID: 16) was highly linked to multiple PRS-MAEs (16%). These results were expected because  
310 the 59 phenotypes (e.g., cognitive and mental traits) are primarily linked to the brain, and  
311 lifestyle factors were largely linked to multiple organ systems (**Fig. 5b** and **Supplementary  
312 eFile 9**). All derived PRS will be returned to UKBB and made available to the community.

313  
314



315  
 316 **Figure 5: The polygenic risk score of the 2024 MAEs and PWAS**  
 317 (a) The incremental  $R^2$  of the PRS derived by PRC-CS to predict the 2024 MAEs in the  
 318 target/test data (i.e., the split2 GWAS). The y-axis indicates the proportions of phenotypic  
 319 variation that the PRS can significantly and additionally explain (i.e., incremental  $R^2$ ). The x-axis  
 320 lists the 8 organ systems. For the brain, we showed the PRS distribution of the significant results  
 321 from the 1791 brain PRS-MAEs; the other organ systems only have one PRS-MAE. (b) The  
 322 PWAS links the PRS-MAEs to the 59 additional phenotypes not used to compute the PRS-MAE  
 323 in the entire UKBB sample (P-value<0.05/2024/59).  
 324



## 325 Discussion

326 This study expands previously established genetic atlases<sup>47,32</sup> by integrating AI-derived  
327 endophenotypes via the 2024 MAEs within the multi-organ framework solely through GWAS  
328 summary statistics. We demonstrate a promising avenue for advancing imaging genetic research  
329 in two key aspects: *i*) integrating AI in imaging genetics and *ii*) exploring human aging and  
330 disease through a multi-organ perspective.

331 By comprehensively depicting the genetic architecture of the 2024 MAEs, we showcased  
332 that AI endophenotypes supported the endophenotype hypothesis<sup>14,15</sup>, in which they showed  
333 lower polygenicity and weaker negative selection effects than the disease diagnosis. First, it may  
334 suggest that these intermediate phenotypes exist along the causal pathway, bridging the gap  
335 between underlying genetics and "exo-phenotypes" like cognitive decline or disease diagnoses in  
336 case/control studies, thus positioned closer to the core etiology and pathology. Secondly, many  
337 of these 2024 MAEs originated from *in vivo* imaging methodologies like magnetic resonance  
338 imaging (MRI). Consequently, they tend to exhibit reduced noise levels (i.e., a higher SNR) in  
339 capturing disease-related effects and are less susceptible to biases, such as misclassification<sup>48</sup>,  
340 case/control-covariate sample bias (e.g., studies matching comorbidities and other factors), and  
341 imbalanced case/control ratios, as evidenced in many GWASs in FinnGen. Especially for the  
342 former, binary traits have a threshold for disease classification, leading to the dichotomization of  
343 individuals into affected and unaffected categories. Thirdly, the 525 DEs often represent  
344 complex diseases highly influenced by multiple genetic and environmental factors. Their  
345 multifaceted nature, involving numerous genes with modest effects and environmental  
346 interactions<sup>49</sup>, can lead to a higher vulnerability to disease onset and clinical symptoms.  
347 Consistent with this observation, we previously also found that one AI- and imaging-derived  
348 subtype of Alzheimer's disease<sup>50</sup> (AD1), but not the binary disease diagnosis, was genetically  
349 correlated with brain age (GM- and WM-BAG)<sup>6</sup>.

350 We observed that brain MAEs were overall more polygenic than MAEs from other organ  
351 systems. Brain disorders are highly polygenic<sup>51</sup>. First, the brain is a highly complex organ with  
352 intricate functions, and disorders affecting it are likely influenced by a larger number of genetic  
353 variants<sup>12,52</sup>. Second, many brain disorders are multifaceted, involving various aspects of brain  
354 structure, function, and connectivity, which can be influenced by various genetic factors<sup>19</sup>.  
355 Additionally, the brain regulates many physiological processes throughout the body, so  
356 disruptions in its function can have widespread effects, potentially involving interactions with  
357 multiple organ systems<sup>4</sup>. In addition, we found that most of the brain MAEs showed negative  
358 selection signatures, including the 9 disease subtype DNEs and 4 brain BAGs; some of the brain  
359 PSCs showed a positive *S* estimate (e.g., for the occipital lobe and subcortical structure,  
360  $S=0.31\pm 0.09$ : [https://labs-laboratory.com/bridgeport/MuSIC/C32\\_18](https://labs-laboratory.com/bridgeport/MuSIC/C32_18)). The anticipated negative  
361 selection signatures of biological age across multiple organs and disease subtypes are expected to  
362 align with our prior findings, which revealed pervasive signatures of natural selection across a  
363 range of complex human traits and functional genomic categories. This negative selection  
364 signature prevents mutations with large deleterious effects from becoming frequent in the  
365 population<sup>53</sup>. The positive selection signatures identified in certain brain PSCs may suggest that  
366 positive selection may also play a role in shaping the genetic architecture of brain structural  
367 networks.

368 The MUTATE atlas uncovered both established and previously undiscovered interactions  
369 concerning human systemic diseases within individual organs and across diverse organ systems.  
370 For example, within the cardiovascular system, the AI-derived MAE, cardiovascular BAG



371 showed both substantial genetic correlation (**Fig. 2**) and bi-directional causality (**Fig. 3 and 4**)  
372 with multiple heart diseases, such as ischaemic heart disease<sup>54</sup>, heart failure<sup>55</sup>, and atrial  
373 fibrillation<sup>56</sup>. Similarly, pulmonary BAG was also causally linked to multiple diseases related to  
374 the lung and respiratory system, including COPD<sup>57</sup> and various forms of asthma<sup>58</sup>. Another  
375 organ-specific connection was observed in neurologic diseases, encompassing conditions such as  
376 AD<sup>59</sup> and various mental disorders<sup>60</sup> linked to several MAEs associated with the brain, notably  
377 several PSCs and WM-BAG. Cross-organ interplay was evidenced for several novel  
378 connections. For instance, the brain PSCs exhibited causal connections to conditions extending  
379 beyond the brain, such as ventral hernia and vein diseases, as well as systemic conditions, like  
380 various forms of diabetes affecting the entire body. In contrast, AD appears to causally impact  
381 multiple BAGs across various human organ systems, including the renal, immune, and metabolic  
382 systems. It's widely recognized that AD, being a complex condition, triggers detrimental effects  
383 that influence several human organ systems<sup>59,61</sup>. Our previous study used imaging genetics to  
384 investigate this multi-organ involvement along the disease continuum<sup>62</sup>. These results highlight  
385 the clinical relevance and interpretation of these AI endophenotypes to quantify individual-level  
386 organ health.

387 Emphasizing preventative strategies for specific chronic diseases is crucial to enhancing  
388 overall multi-organ health. Our MAEs present opportunities as novel instruments for selecting  
389 populations in clinical trials and facilitating therapeutic development. AD and various forms of  
390 diabetes exemplify disease endpoints significantly impacting multiple human organ systems. AD  
391 stands as the leading cause of dementia in older adults, presenting a persistent challenge in  
392 medicine despite numerous pharmacotherapeutic clinical trials. These trials have included  
393 interventions, such as anti-amyloid drugs<sup>63,64</sup> and anti-tau drugs.<sup>65</sup> The complexity and  
394 multifaceted nature of the underlying neuropathological processes may account for the lack of  
395 effective treatments. We call on the scientific community to embrace various mechanistic  
396 hypotheses to elucidate AD pathogenesis beyond amyloid and tau<sup>66,67</sup>. Likewise, the complexity  
397 of diabetes, with its various contributing factors, renders prevention challenging<sup>68</sup>. Moreover,  
398 diabetes often coexists with other chronic conditions affecting multiple organ systems, such as  
399 cardiovascular diseases, hypertension, and dyslipidemia<sup>69</sup>. Successful prevention strategies  
400 require a holistic approach, encompassing lifestyle adjustments, education, healthcare access,  
401 and societal considerations.

402

## 403 **Limitation**

404 This study presents several limitations. Primarily, our analyses were centered solely on GWAS  
405 summary statistics derived from individuals of European ancestries. Future investigations should  
406 extend these findings to diverse ethnic groups, particularly those that are underrepresented, to  
407 ascertain broader applicability. This necessitates the research community's commitment to  
408 embracing open science in AI and genetics. Secondly, the computational genomics statistical  
409 methods utilized in this research rely on several underlying statistical assumptions, which could  
410 potentially be violated and introduce bias. We mitigated bias by employing multiple  
411 methodologies to compute heritability, genetic correlation, and causality to address this concern.  
412 Additionally, we conducted thorough sensitivity checks, and the detailed results are provided  
413 accordingly. Additionally, our analysis was limited by the lack of individual-level genotype data  
414 from FinnGen and PGC, highlighting the need for future studies utilizing individual-level data to  
415 validate our empirical findings. Finally, our study recognizes a tradeoff between clinical  
416 interpretability and the detection of genetic associations when using AI-derived phenotypes.

417

418 **Outlook**

419 In summary, we introduced the MUTATE genetic atlas to comprehensively comprehend the  
420 genetic architecture of AI endophenotypes and chronic diseases in multi-organ science. This  
421 investigation underscores the potential of integrating AI into genetic research and supports a  
422 comprehensive approach to investigating human diseases within a multi-organ paradigm.

## 423 **Methods**

### 424 **Method 1: GWAS summary statistics**

425 The present study solely utilized GWAS summary statistics; no individual-level data were used.  
426 We downloaded the GWAS summary statistics from three web portals for the 2024 MAEs, 521  
427 DEs from FinnGen, and 4 DEs from PGC, respectively.

428

### 429 **UKBB**

430 UKBB is a population-based study of approximately 500,000 people recruited from the United  
431 Kingdom between 2006 and 2010. The UKBB study has ethical approval, and the ethics  
432 committee is detailed here: [https://www.ukbiobank.ac.uk/learn-more-about-uk-](https://www.ukbiobank.ac.uk/learn-more-about-uk-biobank/governance/ethics-advisory-committee)  
433 [biobank/governance/ethics-advisory-committee](https://www.ukbiobank.ac.uk/learn-more-about-uk-biobank/governance/ethics-advisory-committee).

434 The GWAS summary statistics for all the 2024 MAEs are publicly available at the  
435 MEDICINE knowledge portal: <https://labs-laboratory.com/medicine>, which focuses on  
436 disseminating scientific findings on imaging genetics and AI methods in multi-organ science.  
437 Specifically, among the 2024 MAEs, 2003 PSCs – at varying scales from C32 to C1024 – were  
438 structural covariance networks derived via the sopNMF method<sup>12</sup>. 9 DNEs<sup>1</sup> captured the  
439 neuroanatomical heterogeneity of four brain diseases (AD1-2, ASD1-3, LLD1-2, and SCZ1-2)  
440 using semi-supervised clustering or representation learning methods<sup>42,62,71,72</sup>. 12 multi-organ  
441 BAGs (GM, WM, FC<sup>6</sup>, multimodal brain BAGs, cardiovascular BAG, eye BAG, hepatic BAG,  
442 immune BAG, musculoskeletal BAG, metabolic BAG, pulmonary BAG, and renal BAG<sup>73</sup>) were  
443 derived from various machine learning models to quantify the individual-level deviation from  
444 typical brain aging due to various pathological effects. Detailed AI methodologies are presented  
445 in **Method 2** for the MAEs, DNEs, and BAGs. All GWASs were performed within European  
446 ancestries and using the GRCh37 human genome assembly; the GWAS model (PLINK<sup>74</sup> for  
447 linear model and fastGWA<sup>75</sup> for linear mixed-effect model), sample sizes, and covariates  
448 included are detailed in the original papers and also in **Supplementary eTable 1a**.

449 Harmonization of GWAS summary statistics across different models and consortia for  
450 various software is crucial, such as aligning the effect allele and the direction of the effect size.  
451 There's currently no established standard in the field for this process, although some advice has  
452 been proposed<sup>76</sup>. Certain software harmonizes data based on the allele frequency of the effect  
453 allele, such as the *TwoSampleMR* package<sup>77</sup> for Mendelian randomization. In our UKBB MAE  
454 GWAS summary data, we harmonized the effect allele as the alternative allele from PLINK and  
455 A1 from fastGWA and provided its corresponding allele frequency. P-value, effect sizes (e.g.,  
456 BETA value and SE), and sample sizes are indicated too. The variant identifier is based on the rs  
457 ID number, not the chromosome number and position number combination.

458

### 459 **FinnGen**

460 The FinnGen<sup>22</sup> study is a research project based in Finland that explores combined genetics and  
461 health registry data to understand the underlying causes and mechanisms behind various disease  
462 endpoints. It particularly emphasizes the genetic basis of diseases in the Finnish population  
463 (>500,000) by conducting extensive GWAS and analyzing large-scale genomic data in  
464 collaboration with multiple research institutions and organizations. FinnGen has generously  
465 made their GWAS results publicly available to the community for research purposes  
466 ([https://www.finnngen.fi/en/access\\_results](https://www.finnngen.fi/en/access_results)).

467 The present study used the GWAS summary statistics version R9 released to the public  
468 on May 11, 2022, after harmonization by the consortium. In the R9 release, FinnGen analyzed  
469 2269 binary and 3 quantitative endpoints from 377,277 individuals and 20,175,454 variants.  
470 Regenie<sup>78</sup> was used to run the GWAS models, including sex, age, 10 PCs, and genotyping batch  
471 as covariates. Genotype imputation was done with the population-specific SISu v4.0 reference  
472 panel. In our analysis, we concentrated solely on binary DEs with case numbers exceeding 5000  
473 to ensure adequate statistical power, given the highly imbalanced case/control ratios. As the  
474 released data were based on the GRCh38 human genome assembly, we lifted the GWAS  
475 summary statistics to the GRCh37 version for all genetic analyses. **Supplementary eTable 1b**  
476 details the included 521 DEs. More details can be found at the FinnGen website:  
477 <https://finngen.gitbook.io/documentation/v/r9/>.

478 The FinnGen team has systematically harmonized the GWAS summary data for the 521  
479 DEs involved. The alternative allele serves as the effect allele. The rsID number represents the  
480 SNP; the chromosome number and position are also shared. The data includes P-values, effect  
481 sizes, and allele frequencies for both the alternative and reference alleles.  
482

### 483 **Psychiatric Genomics Consortium**

484 PGC<sup>23</sup> is an international coalition of researchers exploring the genetic underpinnings of  
485 psychiatric disorders and beyond. This collaborative effort unites scientists globally to examine  
486 and decipher extensive genomic datasets concerning various brain diseases. The primary goal of  
487 PGC involves uncovering and comprehending the genetic elements that contribute to various  
488 psychiatric disorders, such as schizophrenia, bipolar disorder, and major depressive disorder. We  
489 downloaded GWAS summary statistics from the PGC website ([https://pgc.unc.edu/for-](https://pgc.unc.edu/for-researchers/download-results/)  
490 [researchers/download-results/](https://pgc.unc.edu/for-researchers/download-results/)) and manually harmonized the data to our Mendelian  
491 randomization analyses to replicate the FinnGen findings.

492 PGC did not harmonize the GWAS summary statistics; the available data information  
493 depends on each study. **Supplementary eTable 1c** details the 4 DEs (AD, ADHD, bipolar  
494 disorder, and schizophrenia) included after the data filtering procedure. First, we ensured that the  
495 study population comprised individuals of European ancestry and, if necessary, lifted the data to  
496 the human genome build assembly GRCh37. Secondly, we excluded two studies where the allele  
497 frequency is unavailable because the *TwoSampleMR* package<sup>77</sup> requires this information to  
498 harmonize the exposure and outcome data (e.g., flip the effect allele and effect size). Thirdly, we  
499 confirmed that the GWAS summary statistics didn't overlap with UKBB data. Specifically, the  
500 AD GWAS summary data<sup>79</sup> explicitly offered a version that excluded participants from UKBB.  
501 In addition, the original dataset lacked a column for the rsID number. To deal with this, we  
502 employed a mapping approach using the chromosome number and position to the dpSNP  
503 database (version 150), which allowed us to obtain the corresponding rsID numbers. All 4 DE  
504 GWAS summary data went through the same harmonization procedure as FinnGen (**Method 3c**)  
505

506

### 507 **Method 2: 2024 multi-organ AI endophenotypes**

#### 508 **(a): The 2003 patterns of structural covariance of the brain**

509 In our earlier study<sup>12</sup>, we utilized the sopNMF method on an extensive and varied brain imaging  
510 MRI dataset ( $N=50,699$ , including data from UKBB) to generate the multi-scale brain PSCs. The  
511 scale C ranges from 32 to 1024, progressively increasing by a factor of 2; 11 PSCs vanished  
512 during models.

513 Biologically, the 2003 PSCs represent data-driven structural networks that co-vary across  
514 brain regions and individuals in a coordinated fashion. Mathematically, the sopNMF method is a  
515 stochastic approximation ("deep learning-analogy") constructed and extended based on  
516 opNMF<sup>80,81</sup>. Consider an imaging dataset comprising  $n$  images, each containing  $d$  voxels. We  
517 represent the data as a matrix  $X$ , where each column corresponds to a flattened image:  $X =$   
518  $[x_1, x_2, \dots, x_n]$ ,  $X \in \mathbb{R}_{\geq 0}^{d \times n}$ . The method factorizes  $X$  into two low-rank matrices  $W \in \mathbb{R}_{\geq 0}^{d \times r}$  and  
519  $H \in \mathbb{R}_{\geq 0}^{r \times n}$ , subject to two important constraints: *i*) non-negativity and *ii*) column-wise  
520 orthonormality. More mathematical details can be referred to the original references<sup>12,80,81</sup> and  
521 **Supplementary eMethod 2a**.

### 522 (b): The 9 dimensional neuroimaging endophenotypes of the brain

523 The nine DNEs captured the neuroanatomical heterogeneity of four brain diseases, including  
524 AD1-2 for AD<sup>62</sup>, ASD1-3 for autism spectrum disorder<sup>42</sup>, LLD1-2 for late-life depression<sup>71</sup>, and  
525 SCZ1-2 for schizophrenia<sup>72</sup>. The underlying AI methodologies involved two different semi-  
526 supervised clustering or representation learning algorithms: Surreal-GAN<sup>82</sup> and HYDRA<sup>83</sup>. Refer  
527 to a review for details of the semi-supervised learning<sup>84</sup>, which primarily seeks the so-called "*I-*  
528 *to-k*" mapping patterns or transformations from reference domains (like healthy controls) to  
529 target domains (such as patients).

530 Surreal-GAN<sup>82</sup> was used to derive AD1-2<sup>62</sup>. It unravels the intrinsic heterogeneity  
531 associated with diseases through a deep representation learning approach. The methodological  
532 innovation, compared to its preceptor Smile-GAN<sup>85</sup>, lies in how Surreal-GAN models disease  
533 heterogeneity: it interprets it as a continuous dimensional representation, ensures a consistent  
534 increase in disease severity within each dimension, and permits the simultaneous presence of  
535 multiple dimensions within the same participant without exclusivity. More mathematical details  
536 are presented in **Supplementary eMethod 2b**.

537 HYDRA<sup>83</sup> was employed to derive the other 7 DNEs. It utilizes a widely adopted  
538 discriminative technique, namely support vector machines (SVM), to establish the "*I-to-k*"  
539 mapping. The model extends multiple linear SVMs to the nonlinear domain by piecing them  
540 together. This approach serves the dual purpose of classification and clustering simultaneously.  
541 Specifically, it creates a convex polytope by amalgamating hyperplanes derived from  $k$  linear  
542 SVMs. This polytope separates the healthy control group from the  $k$  subpopulations within the  
543 patient group. Conceptually, each face of this convex polytope can be likened to encoding each  
544 subtype (categorical trait) or dimension (continuous trait), capturing distinctive disease effects  
545 (Refer to **Supplementary eMethod 2c**).

### 546 (c): The 12 biological age gaps of nine human organ systems

547 The nine multi-organ BAGs (brain, cardiovascular, eye, hepatic, immune, musculoskeletal,  
548 metabolic, pulmonary, and renal) were derived from a previous study<sup>5</sup> that used AI to predict the  
549 chronological age of healthy individuals without chronic medical conditions: AI-predicted age –  
550 chronological age. Using a 20-fold cross-validation procedure, we applied the model for each  
551 organ system, employing a linear support vector machine. Before training each model iteration,  
552 standardization was applied to measures (excluding categorical variables) within the training set.  
553 The model was solved using sequential minimal optimization with a gap tolerance of 0.001. The  
554 support vector regression settings were adjusted for optimization, adhering to established  
555 principles in the field<sup>86</sup>.



558           Alongside the nine organ BAGs, we previously derived three multimodal brain BAGs  
559 (GM, WM, and FC-IDP) using features from gray matter (GM), white matter (WM), and  
560 functional connectivity (FC) in MRI scans<sup>6</sup>. We systematically compared four machine learning  
561 models: SVR, LASSO regression, multilayer perceptron, and a five-layer neural network. We  
562 employed nested cross-validation (CV) and included an independent test dataset<sup>87</sup> for a fair  
563 comparison across different models and MRI modalities. This process involved an outer loop CV  
564 with 100 repeated random splits: 80% for training and validation and 20% for testing. Within the  
565 inner loop, a 10-fold CV was utilized for hyperparameter tuning. Furthermore, we reserved an  
566 independent test dataset, which was kept unseen until the fine-tuning of the machine learning  
567 models<sup>88</sup> (e.g., hyperparameters for SVR) was completed.  
568

### 569 **Method 3: Genetic analyses based on GWAS summary statistics**

#### 570 **(a): The genetic architecture of the 2024 MAEs and 525 DEs**

571 Primarily, we used SBayesS<sup>39</sup> to estimate three sets of parameters that fully unveil the genetic  
572 architecture of the 2024 MAEs and 525 DEs. SBayesS is an expanded approach capable of  
573 estimating three essential parameters characterizing the genetic architecture of complex traits  
574 through a Bayesian mixed linear model<sup>89</sup>. This method only requires GWAS summary statistics  
575 of the SNPs and LD information from a reference sample. These parameters include SNP-based  
576 heritability ( $h_{SNP}^2$ ), polygenicity ( $\pi$ ), and the relationship between minor allele frequency (MAF)  
577 and effect size ( $S$ ). We used the software pre-computed sparse LD correlation matrix derived  
578 from the European ancestry by Zeng et al.<sup>39</sup>. More mathematical details can be found in the  
579 original paper from Zeng et al.<sup>39</sup>. We ran the *gctb* command<sup>89</sup> using the argument *--sbayes S*, and  
580 left all other arguments by default. When applying SBayesS to the 2025 MAEs and 525 DEs  
581 summary data, we found that 18 DEs failed to converge in the MCMC sampling, which may be  
582 due to LD differences between FinnGen and UKBB samples (the latter was used as the LD  
583 reference in SBayesS).

584           To benchmark different methods used in the field for SNP-based heritability estimates,  
585 we also employed two other methods based on GWAS summary data: *i*) LDSC<sup>28</sup> and *ii*)  
586 SumHer<sup>33</sup>. LDSC relies on the principle that the correlation between SNP effect sizes and  
587 linkage disequilibrium with neighboring SNPs can be used to estimate the proportion of  
588 heritability explained by all SNPs using GWAS summary data. For LDSC, we used the  
589 precomputed LD scores from the 1000 Genomes of European ancestry. All other parameters  
590 were set to default in the software. After merging the GWAS summary statistics, we chose the  
591 1000 Genomes reference panel for fair comparisons between the two studies and ensured that  
592 most SNPs were included in the analyses. For example, for the DE  
593 (RX\_PARACETAMOL\_NSAID), after merging with the reference panel LD, 1,171,361  
594 remained. For the first MAE (C32\_1), 1,092,510 SNPs remained after the same merging  
595 procedure. Furthermore, FinnGen didn't provide the original genotype data; they only shared the  
596 LD information via the LDstore software but did not provide the allele information.  
597 Consequently, we cannot generate in-sample LD scores using the LDSC software. Finally, a  
598 prior investigation<sup>90</sup> showcased the robustness of LDSC concerning the selection of LD  
599 reference panels – multi-ethnic European, Finnish-only, non-Finnish European from 1000  
600 Genomes Phase 3 data, and FINRISK Finnish reference panel – regarding heritability estimates  
601 in four lipid traits within a Finnish population.



602 For SumHer, we used the BLD-LDAK model , as the software suggested. BLD-LDAK  
603 stands for "Bayesian LD-adjusted Kinship," where LD-adjusted kinship refers to the calculation  
604 of genetic relatedness between individuals using information about the correlation of alleles  
605 between nearby SNPs (linkage disequilibrium). We used the software-provided tagging file,  
606 generated from 2000 white British individuals, as a reference panel suggested by the software for  
607 European ancestry groups. The HapMap3 data ([https://www.broadinstitute.org/medical-and-](https://www.broadinstitute.org/medical-and-population-genetics/hapmap-3)  
608 [population-genetics/hapmap-3](https://www.broadinstitute.org/medical-and-population-genetics/hapmap-3)) merged with the tested GWAS summary SNPs. Similarly, we  
609 ensured sufficient SNPs remained after merging with the reference panel. All other parameters  
610 were set to default. SumHer differs from LDSC in several ways: *i*) it models inflation  
611 multiplicatively, whereas LDSC uses an additive approach; *ii*) it accounts for uneven LD patterns  
612 and incorporates MAF on SNP effect; and *iii*) it utilizes a restricted maximum likelihood  
613 solver rather than regression to estimate the  $h_{SNP}^2$ .

614  
615 **(b): Genetic correlation:** We used three different methods to compute the MAE-DE pairwise  
616 ( $N=2024 \times 525=1,062,600$ ) genetic correlations ( $r_g$ ): *i*) LDSC<sup>28</sup>, *ii*) GNOVA<sup>34</sup>, and *iii*) HDL<sup>38</sup>.

617 An earlier study<sup>92</sup> highlighted the significance of selecting an appropriate LD score  
618 reference panel for genetic correlation estimates based on summary statistics. We generated the  
619 same reference panel for LD scores across the three software for a fair comparison. For LDSC,  
620 we used the precomputed LD scores from the 1000 Genomes of European ancestry provided by  
621 the software. All other parameters were set by default. To employ GNOVA, we created the LD  
622 scores utilizing the 1000 Genomes of European ancestry using the `--save-ld` argument within the  
623 `gnova.py` script. For HDL, we used the provided scripts from HDL to generate the LD scores  
624 using the same 1000 Genomes of European ancestry  
625 (<https://github.com/zhenin/HDL/wiki/Build-a-reference-panel>).

626 Through our analysis, we found that the three packages have different levels of model  
627 convergence rates, which is critical for future applications as these open-source packages claim  
628 to advance genetic research. In particular, we found that LDSC (1,062,577/1,062,600) and  
629 GNOVA (1,062,600/1,062,600) converged for most of the tested MAE-DE pairs, whereas HDL  
630 failed a substantial proportion of the analyses, leading to only 59,291 out of the 1,062,600 MAE-  
631 DE pairs (refer to the raised issue: <https://github.com/zhenin/HDL/issues/30>). Therefore, in **Fig.**  
632 **2**, we presented common significant results after Bonferroni corrections from the LDSC and  
633 GNOVA, resulting in 133 and 45 significant signals corrected on *i*) the number of MAEs and *ii*)  
634 the number of MAEs and DEs.

635  
636 **(c): Two-sample bidirectional Mendelian randomization:** We employed a bidirectional, two-  
637 sample Mendelian randomization using the *TwoSampleMR* package<sup>77</sup> to infer the causal  
638 relationships between the 2024 MAEs, 521 DEs from FinnGen, and 4 brain DEs from PGC.

639 The forward Mendelian randomization examined causality from the 2024 MAEs to the  
640 525 DEs, while the inverse analysis investigated causality from the 525 DEs to the 2024 MAEs.  
641 The *TwoSampleMR* package<sup>77</sup> applied five different Mendelian randomization methods. We  
642 presented the significant findings after the Bonferroni correction using the inverse variance  
643 weighted (IVW) estimator, verifying that the correction remained significant in at least one of  
644 the other four estimators (Egger, weighted median, simple mode, and weighted mode  
645 estimators). For the significant signals, we performed several sensitivity analyses. First, a  
646 heterogeneity test was performed to check for violating the IV assumptions. Horizontal  
647 pleiotropy was estimated to navigate the violation of the IV's exclusivity assumption<sup>93</sup> using a

648 funnel plot, single-SNP Mendelian randomization approaches, and Mendelian randomization  
649 Egger estimator . Moreover, the leave-one-out analysis excluded one instrument (SNP) at a time  
650 and assessed the sensitivity of the results to individual SNP.

651 Critically, to enhance transparency and reproducibility, we followed a systematic  
652 procedure guided by the STROBE-MR Statement<sup>94</sup> in conducting all causality analyses. This  
653 comprehensive approach encompassed the selection of exposure and outcome variables,  
654 reporting full sets of statistics, and implementing sensitivity checks to identify potential  
655 violations of underlying assumptions. First, we performed an unbiased quality check on the  
656 GWAS summary statistics. Notably, the absence of population overlapping bias<sup>29</sup> was  
657 confirmed, given that FinnGen and UKBB participants largely represent European ancestry  
658 populations without explicit overlap. For the four PGC DEs, we ensured that no UKBB  
659 participants were included in the GWAS summary data. Furthermore, all GWAS summary  
660 statistics were based on or lifted to GRCh37. Subsequently, we selected the effective exposure  
661 variables by assessing the statistical power of the exposure GWAS summary statistics in terms of  
662 instrumental variables (IVs), ensuring that the number of IVs exceeded 8 before harmonizing the  
663 data. Crucially, the function "*clump\_data*" was applied to the exposure GWAS data, considering  
664 LD. The function "*harmonise\_data*" was then used to harmonize the GWAS summary statistics  
665 of the exposure and outcome variables. This overall resulted in a smaller number (< 525 DEs or  
666 2024 MAEs) of effective exposure/outcome variables in both forward and inverse Mendelian  
667 randomization analyses, as certain GWAS summary data did not have enough IVs.

668  
669 **(d): PRS calculation:** PRS calculation used the GWAS summary statistics from the split-sample  
670 sensitivity analysis from our previous studies<sup>12,6,4,1</sup>. We established PRS weights using split1  
671 GWAS data as the base/training set, while the split2 GWAS summary statistics were used as the  
672 target/testing data. Details of the quality control (QC) procedures are shown in our previous  
673 studies<sup>12,6,4,1</sup>. Following the QC procedures, PRS for the split2 group was computed using PRS-  
674 CS<sup>45</sup>. PRS-CS infers posterior SNP effect sizes under continuous shrinkage priors using GWAS  
675 summary statistics and an LD reference panel (i.e., UKBB reference). To ascertain the most  
676 suitable PRS, we conducted a linear regression encompassing different P-value thresholds  
677 (0.001, 0.05, 0.1, 0.2, 0.3, 0.4, 0.5), while controlling for age, sex, intracranial volume (if  
678 applicable), and the forty genetic principal components. The optimal P-value threshold for PRS-  
679 MAE was determined based on the highest incremental  $R^2$ .

680 After determining the optimal model, we applied the model to the entire UKBB sample  
681 (~500k individuals). We then performed a PWAS to link the 2024 PRS-MAEs and 59 additional  
682 phenotypes (**Supplementary eTable 5**) not used to compute the PRS-MAE to avoid the circular  
683 bias<sup>46</sup>. The 59 phenotypes include cognitive scores (e.g., fluid intelligence score; Field ID:  
684 20016, mental traits (e.g., fed-up feelings; Filed ID: 1960), and lifestyle factors (e.g., tea intake;  
685 Filed ID: 1488). A linear regression was built considering the following covariates: sex (Field  
686 ID: 31), smoking status (Field ID: 20116), weight (Field ID: 21002), standing height (Field ID:  
687 50), waist circumference (Field ID: 48), age at recruitment (Field ID: 21022), and first 40 genetic  
688 principal components (Field ID: 22009).

689  
690

## 691 **Data Availability**

692 The results of the MUTATE atlas are disseminated at the MUTATE knowledge portal:  
693 <https://labs-laboratory.com/mutate>. The GWAS summary statistics for the 2024 MAEs can be  
694 accessed publicly through the MEDICINE knowledge portal: [https://labs-](https://labs-laboratory.com/medicine)  
695 [laboratory.com/medicine](https://labs-laboratory.com/medicine) and the BRIDGEPORT knowledge portal: [https://labs-](https://labs-laboratory.com/bridgeport)  
696 [laboratory.com/bridgeport](https://labs-laboratory.com/bridgeport). The GWAS summary statistics for the 521 DEs from FinnGen are  
697 publicly available at: <https://finngen.gitbook.io/documentation/v/r9/>. The GWAS summary  
698 statistics for the 4 DEs from PGC are publicly available at: [https://pgc.unc.edu/for-](https://pgc.unc.edu/for-researchers/download-results/)  
699 [researchers/download-results/](https://pgc.unc.edu/for-researchers/download-results/). The study used only GWAS summary statistics rather than  
700 individual-level data from the UK Biobank. However, the 2024 MAE GWAS data was initially  
701 derived from previous studies conducted under Application Numbers 35148 and 60698 from the  
702 UK Biobank.

## 703 **Code Availability**

704 The software and resources used in this study are all publicly available:

- 705 • *GCTB*: <https://cnsgenomics.com/software/gctb/#Overview>, SNP-based heritability,  
706 polygenicity, and MAF/effect size ratio
- 707 • *LDSC*: <https://github.com/bulik/ldsc>, SNP-based heritability and genetic correlation
- 708 • *SumHer*: <https://dougsspeed.com/sumher/>, SNP-based heritability
- 709 • *GNOVA*: <https://github.com/xtonyjiang/GNOVA>, genetic correlation
- 710 • *HDL*: <https://github.com/zhenin/HDL>, genetic correlation
- 711 • *TwoSampleMR*: <https://mrcieu.github.io/TwoSampleMR/index.html>, Mendelian  
712 randomization
- 713 • PRS-CS: <https://github.com/getian107/PRScs>, PRS
- 714 • Surreal-GAN: <https://github.com/zhijian-yang/SurrealGAN>, to derive AD1 and AD2
- 715 • HYDRA: <https://github.com/anbai106/mlni>, to derive LLD1-2, SCZ1-2, ASD1-3, and  
716 GM-, WM-, FC-BAG
- 717 • sopNMF: <https://github.com/anbai106/SOPNMF>, to derive the 2003 brain PSCs
- 718 • BioAge: <https://github.com/yetianmed/BioAge>, to derive the 9 multi-organ BAGs
- 719

720 **Competing Interests**

721 None

722

723 **Authors' contributions**

724 Dr. Wen has full access to all the study data and is responsible for its integrity and accuracy.

725 *Study concept and design:* W.J

726 *Acquisition, analysis, or interpretation of data:* W.J

727 *Drafting of the manuscript:* W.J

728 *Critical revision of the manuscript for important intellectual content:* All authors

729 *Statistical analysis:* W.J



## 730 **References**

- 731 1. Wen, J. *et al.* Neuroimaging-AI Endophenotypes of Brain Diseases in the General  
732 Population: Towards a Dimensional System of Vulnerability. 2023.08.16.23294179  
733 Preprint at <https://doi.org/10.1101/2023.08.16.23294179> (2023).
- 734 2. Trubetskoy, V. *et al.* Mapping genomic loci implicates genes and synaptic biology in  
735 schizophrenia. *Nature* **604**, 502–508 (2022).
- 736 3. Kendler, K. & Neale, M. Endophenotype: a conceptual analysis. *Mol Psychiatry* **15**, 789–  
737 797 (2010).
- 738 4. Wen, J. *et al.* The Genetic Architecture of Biological Age in Nine Human Organ Systems.  
739 *medRxiv* 2023.06.08.23291168 (2023) doi:10.1101/2023.06.08.23291168.
- 740 5. Tian, Y. E. *et al.* Heterogeneous aging across multiple organ systems and prediction of  
741 chronic disease and mortality. *Nat Med* 1–11 (2023) doi:10.1038/s41591-023-02296-6.
- 742 6. Wen, J. *et al.* The genetic architecture of multimodal human brain age. *Nat Commun* **15**,  
743 2604 (2024).
- 744 7. Zhao, B. *et al.* Heart-brain connections: Phenotypic and genetic insights from magnetic  
745 resonance images. *Science* **380**, abn6598 (2023).
- 746 8. McCracken, C. *et al.* Multi-organ imaging demonstrates the heart-brain-liver axis in UK  
747 Biobank participants. *Nat Commun* **13**, 7839 (2022).
- 748 9. Nie, C. *et al.* Distinct biological ages of organs and systems identified from a multi-omics  
749 study. *Cell Reports* **38**, 110459 (2022).
- 750 10. Liu, Y. *et al.* Genetic architecture of 11 organ traits derived from abdominal MRI using  
751 deep learning. *eLife* **10**, e65554 (2021).

- 752 11. Oh, H. S.-H. *et al.* Organ aging signatures in the plasma proteome track health and disease.  
753 *Nature* **624**, 164–172 (2023).
- 754 12. Wen, J. *et al.* Genomic loci influence patterns of structural covariance in the human brain.  
755 *Proceedings of the National Academy of Sciences* **120**, e2300842120 (2023).
- 756 13. Hodson, R. Precision medicine. *Nature* **537**, S49–S49 (2016).
- 757 14. Gottesman, I. I. & Gould, T. D. The endophenotype concept in psychiatry: etymology and  
758 strategic intentions. *Am J Psychiatry* **160**, 636–645 (2003).
- 759 15. Cannon, T. D. & Keller, M. C. Endophenotypes in the Genetic Analyses of Mental  
760 Disorders. *Annual Review of Clinical Psychology* **2**, 267–290 (2006).
- 761 16. Rajpurkar, P., Chen, E., Banerjee, O. & Topol, E. J. AI in health and medicine. *Nat Med* **28**,  
762 31–38 (2022).
- 763 17. Bycroft, C. *et al.* The UK Biobank resource with deep phenotyping and genomic data.  
764 *Nature* **562**, 203–209 (2018).
- 765 18. Miller, K. L. *et al.* Multimodal population brain imaging in the UK Biobank prospective  
766 epidemiological study. *Nature Neuroscience* **19**, 1523–1536 (2016).
- 767 19. Elliott, L. T. *et al.* Genome-wide association studies of brain imaging phenotypes in UK  
768 Biobank. *Nature* **562**, 210–216 (2018).
- 769 20. Sun, B. B. *et al.* Plasma proteomic associations with genetics and health in the UK  
770 Biobank. *Nature* **622**, 329–338 (2023).
- 771 21. Dhindsa, R. S. *et al.* Rare variant associations with plasma protein levels in the UK  
772 Biobank. *Nature* **622**, 339–347 (2023).
- 773 22. Kurki, M. I. *et al.* FinnGen provides genetic insights from a well-phenotyped isolated  
774 population. *Nature* **613**, 508–518 (2023).

- 775 23. O'Donovan, M. C. What have we learned from the Psychiatric Genomics Consortium.  
776 *World Psychiatry* **14**, 291–293 (2015).
- 777 24. Buniello, A. *et al.* The NHGRI-EBI GWAS Catalog of published genome-wide association  
778 studies, targeted arrays and summary statistics 2019. *Nucleic Acids Res* **47**, D1005–D1012  
779 (2019).
- 780 25. Elsworth, B. *et al.* The MRC IEU OpenGWAS data infrastructure. 2020.08.10.244293  
781 Preprint at <https://doi.org/10.1101/2020.08.10.244293> (2020).
- 782 26. Watanabe, K. *et al.* A global overview of pleiotropy and genetic architecture in complex  
783 traits. *Nat Genet* **51**, 1339–1348 (2019).
- 784 27. Shen, L. & Thompson, P. M. Brain Imaging Genomics: Integrated Analysis and Machine  
785 Learning. *Proceedings of the IEEE* **108**, 125–162 (2020).
- 786 28. Bulik-Sullivan, B. K. *et al.* LD Score regression distinguishes confounding from  
787 polygenicity in genome-wide association studies. *Nat Genet* **47**, 291–295 (2015).
- 788 29. Sanderson, E. *et al.* Mendelian randomization. *Nat Rev Methods Primers* **2**, 1–21 (2022).
- 789 30. Bowden, J., Davey Smith, G. & Burgess, S. Mendelian randomization with invalid  
790 instruments: effect estimation and bias detection through Egger regression. *Int J Epidemiol*  
791 **44**, 512–525 (2015).
- 792 31. Open science. *Nature* **550**, 7–8 (2017).
- 793 32. Bulik-Sullivan, B. *et al.* An atlas of genetic correlations across human diseases and traits.  
794 *Nat Genet* **47**, 1236–1241 (2015).
- 795 33. Speed, D. & Balding, D. J. SumHer better estimates the SNP heritability of complex traits  
796 from summary statistics. *Nat Genet* **51**, 277–284 (2019).

- 797 34. Lu, Q. *et al.* A Powerful Approach to Estimating Annotation-Stratified Genetic Covariance  
798 via GWAS Summary Statistics. *The American Journal of Human Genetics* **101**, 939–964  
799 (2017).
- 800 35. Smith, G. D. & Ebrahim, S. ‘Mendelian randomization’: can genetic epidemiology  
801 contribute to understanding environmental determinants of disease? *Int J Epidemiol* **32**, 1–  
802 22 (2003).
- 803 36. Davey Smith, G. & Hemani, G. Mendelian randomization: genetic anchors for causal  
804 inference in epidemiological studies. *Hum Mol Genet* **23**, R89-98 (2014).
- 805 37. Pierce, B. L. & Burgess, S. Efficient design for Mendelian randomization studies:  
806 subsample and 2-sample instrumental variable estimators. *Am J Epidemiol* **178**, 1177–1184  
807 (2013).
- 808 38. Ning, Z., Pawitan, Y. & Shen, X. High-definition likelihood inference of genetic  
809 correlations across human complex traits. *Nat Genet* **52**, 859–864 (2020).
- 810 39. Zeng, J. *et al.* Widespread signatures of natural selection across human complex traits and  
811 functional genomic categories. *Nat Commun* **12**, 1164 (2021).
- 812 40. Evans, L. M. *et al.* Comparison of methods that use whole genome data to estimate the  
813 heritability and genetic architecture of complex traits. *Nat Genet* **50**, 737–745 (2018).
- 814 41. Ojavee, S. E., Kutalik, Z. & Robinson, M. R. Liability-scale heritability estimation for  
815 biobank studies of low-prevalence disease. *The American Journal of Human Genetics* **109**,  
816 2009–2017 (2022).
- 817 42. Hwang, G. *et al.* Assessment of Neuroanatomical Endophenotypes of Autism Spectrum  
818 Disorder and Association With Characteristics of Individuals With Schizophrenia and the  
819 General Population. *JAMA Psychiatry* (2023) doi:10.1001/jamapsychiatry.2023.0409.

- 820 43. Makowski, C. *et al.* Discovery of genomic loci of the human cerebral cortex using  
821 genetically informed brain atlases. *8* (2022).
- 822 44. Matoba, N., Love, M. I. & Stein, J. L. Evaluating brain structure traits as endophenotypes  
823 using polygenicity and discoverability. *Human Brain Mapping* **43**, 329–340 (2022).
- 824 45. Ge, T., Chen, C.-Y., Ni, Y., Feng, Y.-C. A. & Smoller, J. W. Polygenic prediction via  
825 Bayesian regression and continuous shrinkage priors. *Nat Commun* **10**, 1776 (2019).
- 826 46. Kriegeskorte, N., Simmons, W. K., Bellgowan, P. S. F. & Baker, C. I. Circular analysis in  
827 systems neuroscience: the dangers of double dipping. *Nat. Neurosci.* **12**, 535–540 (2009).
- 828 47. Sakaue, S. *et al.* A cross-population atlas of genetic associations for 220 human  
829 phenotypes. *Nat Genet* **53**, 1415–1424 (2021).
- 830 48. Lee, S. H. *et al.* Genetic relationship between five psychiatric disorders estimated from  
831 genome-wide SNPs. *Nat Genet* **45**, 984–994 (2013).
- 832 49. Hunter, D. J. Gene–environment interactions in human diseases. *Nat Rev Genet* **6**, 287–298  
833 (2005).
- 834 50. Wen, J. *et al.* Genetic, clinical underpinnings of subtle early brain change along  
835 Alzheimer’s dimensions. 2022.09.16.508329 Preprint at  
836 <https://doi.org/10.1101/2022.09.16.508329> (2022).
- 837 51. THE BRAINSTORM CONSORTIUM *et al.* Analysis of shared heritability in common  
838 disorders of the brain. *Science* **360**, eaap8757 (2018).
- 839 52. Smith, S. M. *et al.* An expanded set of genome-wide association studies of brain imaging  
840 phenotypes in UK Biobank. *Nat Neurosci* **24**, 737–745 (2021).
- 841 53. Walsh, B. & Lynch, M. *Evolution and Selection of Quantitative Traits*. (Oxford University  
842 Press, 2018).

- 843 54. Plackett, B. A graphical guide to ischaemic heart disease. *Nature* **594**, S3–S3 (2021).
- 844 55. Peisker, F. *et al.* Mapping the cardiac vascular niche in heart failure. *Nat Commun* **13**, 3027  
845 (2022).
- 846 56. Brundel, B. J. J. M. *et al.* Atrial fibrillation. *Nat Rev Dis Primers* **8**, 1–23 (2022).
- 847 57. Barnes, P. J. *et al.* Chronic obstructive pulmonary disease. *Nat Rev Dis Primers* **1**, 1–21  
848 (2015).
- 849 58. Holgate, S. T. *et al.* Asthma. *Nat Rev Dis Primers* **1**, 1–22 (2015).
- 850 59. Ballard, C. *et al.* Alzheimer’s disease. *The Lancet* **377**, 1019–1031 (2011).
- 851 60. Marshall, M. The hidden links between mental disorders. *Nature* **581**, 19–21 (2020).
- 852 61. Eiser, A. R. & Fulop, T. Alzheimer’s Disease Is a Multi-Organ Disorder: It May Already  
853 Be Preventable. *J Alzheimers Dis* **91**, 1277–1281 (2023).
- 854 62. Wen, J. *et al.* Genetic, clinical underpinnings of subtle early brain change along  
855 Alzheimer’s dimensions. 2022.09.16.508329 Preprint at  
856 <https://doi.org/10.1101/2022.09.16.508329> (2022).
- 857 63. Guthrie, H. *et al.* Safety, Tolerability, and Pharmacokinetics of Crenezumab in Patients  
858 with Mild-to-Moderate Alzheimer’s Disease Treated with Escalating Doses for up to  
859 133 Weeks. *J Alzheimers Dis* **76**, 967–979 (2020).
- 860 64. Sevigny, J. *et al.* The antibody aducanumab reduces A $\beta$  plaques in Alzheimer’s disease.  
861 *Nature* **537**, 50–56 (2016).
- 862 65. Congdon, E. E. & Sigurdsson, E. M. Tau-targeting therapies for Alzheimer disease. *Nat Rev*  
863 *Neurol* **14**, 399–415 (2018).
- 864 66. Jack, C. R. *et al.* Tracking pathophysiological processes in Alzheimer’s disease: an updated  
865 hypothetical model of dynamic biomarkers. *Lancet Neurol* **12**, 207–216 (2013).



- 866 67. Frisoni, G. B. *et al.* The probabilistic model of Alzheimer disease: the amyloid hypothesis  
867 revised. *Nat Rev Neurosci* **23**, 53–66 (2022).
- 868 68. Tomic, D., Shaw, J. E. & Magliano, D. J. The burden and risks of emerging complications  
869 of diabetes mellitus. *Nat Rev Endocrinol* **18**, 525–539 (2022).
- 870 69. DeFronzo, R. A. *et al.* Type 2 diabetes mellitus. *Nat Rev Dis Primers* **1**, 1–22 (2015).
- 871 70. Yang, Z. *et al.* Gene-SGAN: discovering disease subtypes with imaging and genetic  
872 signatures via multi-view weakly-supervised deep clustering. *Nat Commun* **15**, 354 (2024).
- 873 71. Wen, J. *et al.* Characterizing Heterogeneity in Neuroimaging, Cognition, Clinical  
874 Symptoms, and Genetics Among Patients With Late-Life Depression. *JAMA Psychiatry*  
875 (2022) doi:10.1001/jamapsychiatry.2022.0020.
- 876 72. Chand, G. B. *et al.* Two distinct neuroanatomical subtypes of schizophrenia revealed using  
877 machine learning. *Brain* **143**, 1027–1038 (2020).
- 878 73. Wen, J. *et al.* The Genetic Architecture of Biological Age in Nine Human Organ Systems.  
879 *medRxiv* 2023.06.08.23291168 (2023) doi:10.1101/2023.06.08.23291168.
- 880 74. Purcell, S. *et al.* PLINK: A Tool Set for Whole-Genome Association and Population-Based  
881 Linkage Analyses. *Am J Hum Genet* **81**, 559–575 (2007).
- 882 75. Jiang, L. *et al.* A resource-efficient tool for mixed model association analysis of large-scale  
883 data. *Nat Genet* **51**, 1749–1755 (2019).
- 884 76. MacArthur, J. A. L. *et al.* Workshop proceedings: GWAS summary statistics standards and  
885 sharing. *Cell Genomics* **1**, (2021).
- 886 77. Hemani, G. *et al.* The MR-Base platform supports systematic causal inference across the  
887 human phenome. *eLife* **7**, e34408 (2018).

- 888 78. Mbatchou, J. *et al.* Computationally efficient whole-genome regression for quantitative and  
889 binary traits. *Nat Genet* **53**, 1097–1103 (2021).
- 890 79. Wightman, D. P. *et al.* A genome-wide association study with 1,126,563 individuals  
891 identifies new risk loci for Alzheimer’s disease. *Nat Genet* **53**, 1276–1282 (2021).
- 892 80. Sotiras, A., Resnick, S. M. & Davatzikos, C. Finding imaging patterns of structural  
893 covariance via Non-Negative Matrix Factorization. *NeuroImage* **108**, 1–16 (2015).
- 894 81. Zhirong Yang & Oja, E. Linear and Nonlinear Projective Nonnegative Matrix  
895 Factorization. *IEEE Trans. Neural Netw.* **21**, 734–749 (2010).
- 896 82. Yang, Z., Wen, J. & Davatzikos, C. Surreal-GAN:Semi-Supervised Representation  
897 Learning via GAN for uncovering heterogeneous disease-related imaging patterns. *ICLR*  
898 (2021).
- 899 83. Varol, E., Sotiras, A. & Davatzikos, C. HYDRA: Revealing heterogeneity of imaging and  
900 genetic patterns through a multiple max-margin discriminative analysis framework.  
901 *NeuroImage* **145**, 346–364 (2017).
- 902 84. Wen, J. *et al.* Subtyping Brain Diseases from Imaging Data. in *Machine Learning for Brain*  
903 *Disorders* (ed. Colliot, O.) 491–510 (Springer US, New York, NY, 2023). doi:10.1007/978-  
904 1-0716-3195-9\_16.
- 905 85. Yang, Z. *et al.* A deep learning framework identifies dimensional representations of  
906 Alzheimer’s Disease from brain structure. *Nat Commun* **12**, 7065 (2021).
- 907 86. Chang, C.-C. & Lin, C.-J. LIBSVM: A library for support vector machines. *ACM Trans.*  
908 *Intell. Syst. Technol.* **2**, 1–27 (2011).

- 909 87. Samper-González, J. *et al.* Reproducible evaluation of classification methods in  
910 Alzheimer’s disease: Framework and application to MRI and PET data. *NeuroImage* **183**,  
911 504–521 (2018).
- 912 88. Wen, J. *et al.* Convolutional neural networks for classification of Alzheimer’s disease:  
913 Overview and reproducible evaluation. *Medical Image Analysis* **63**, 101694 (2020).
- 914 89. Zeng, J. *et al.* Signatures of negative selection in the genetic architecture of human complex  
915 traits. *Nat Genet* **50**, 746–753 (2018).
- 916 90. Hautakangas, H. LD Score regression for estimating and partitioning heritability of lipid  
917 levels in the Finnish population. (University of Helsinki, Helsinki, 2018).
- 918 91. Speed, D., Holmes, J. & Balding, D. J. Evaluating and improving heritability models using  
919 summary statistics. *Nat Genet* **52**, 458–462 (2020).
- 920 92. Zhang, Y. *et al.* Comparison of methods for estimating genetic correlation between  
921 complex traits using GWAS summary statistics. *Brief Bioinform* **22**, bbaa442 (2021).
- 922 93. Bowden, J. *et al.* A framework for the investigation of pleiotropy in two-sample summary  
923 data Mendelian randomization. *Stat Med* **36**, 1783–1802 (2017).
- 924 94. Skrivankova, V. W. *et al.* Strengthening the Reporting of Observational Studies in  
925 Epidemiology Using Mendelian Randomization: The STROBE-MR Statement. *JAMA* **326**,  
926 1614–1621 (2021).
- 927

928 **Acknowledgment**

929 We sincerely thank the UK Biobank (<https://www.ukbiobank.ac.uk/>), FinnGen  
930 (<https://www.finngen.fi/en>), and PGC (<https://pgc.unc.edu/>) team for their invaluable  
931 contribution to advancing clinical research in our field.